

Session IC (2) – Thermography

Chairman – Mr C Pearson

11.15 Finite Element Simulation of Thermography Non-destructive Testing for Gear Inspection

Author - Xin Wang, Kar Weng Ng, Jong Boon Ooi, Jee Hou Ho, ChingSeong Tan and Anthony Guo

Thermography non-destructive inspection is widely used as a no-destructive testing method in a variety of applications. In this paper, finite element model is used for simulation of thermography inspection for gear inspection, which could allow us to predict its behaviour before advance to the experiment. The 3-D gear model is build. The defects with different dimension and depth gear are simulating. Surface temperature distribution of tested object is computed. When the heat distribution is distorted due to the crack appear, it has a temperature drop. The abnormal heat path emphasizes the cracked area. In simulation, three types of materials are chosen. Their material characteristic is high, moderate and low in thermal conductivity respectively. Their thermal conductivity directly influences the heat flow rate on the specimen and time for the heat propagation. The comparisons are made between these kinds of materials to study their behavior on thermography inspection.

Finite Element Simulation of Thermography Non-destructive Testing for Gear Inspection

*Xin Wang, *Kar Weng Ng, *Ying Pio Lim, *Jong Boon Ooi,
*Jee-Hou Ho, *Ching Seong Tan, **Anthony Guo

*University Tunku Abdul Rahman
** Monash University

Abstract

Thermography non-destructive inspection is widely used as a non-destructive testing method in a variety of applications. This paper describes the application of finite element method for simulation of thermography inspection in gear inspection. This enables the prediction of its behavior in advance to the experiment. The 3-D gear was modeled and simulated using finite element method. The defects with different dimension and depth gear were simulated. Surface temperature distribution of gear for testing was computed. Distortion of heat distribution signifies the crack appearance since there is a temperature drop in the crack region. The abnormal heat path emphasizes the cracked area. In simulation, three types of materials are chosen. Their material characteristic is high, moderate and low in thermal conductivity respectively. Their thermal conductivity directly influences the heat flow rate on the specimen and time for the heat propagation. The comparisons are made between these kinds of materials to study their behavior on thermography inspection.

1. Introduction

Thermography is related to infrared imaging science which produces pictures of the radiation base on the temperature. Infrared thermography has a wide range of application ⁽¹⁾, which includes structural inspection ⁽²⁻⁴⁾, microelectronic imaging ⁽⁵⁾, diffusivity measurement ⁽⁷⁾, aerospace ⁽⁷⁻⁹⁾ and medical applications ⁽¹⁰⁻¹¹⁾. The radiation of the infrared ranging between 900 to 14,000 nanometres of the electromagnetic spectrum can be detected using the thermographic camera and produce images that represent heat wave contour. Ideally, a gear specimen with a perfect heat conducting medium and a simple boundary condition could create a geometrically predictable path (trajectory) of the heat flows. This technique uses a heating element to produce a localized heating spot from which heat diffuses radially from the source. Heat flow along the surface of the gear would be affected by impurities or flaws causing distortion of the heat flow pattern. Simulation of heat flow shows various heat distributions along the surface with the interference present. The presence of crack in the surface of the specimen allows the detection of the imperfect surface due to disturbance the heat flows. The purpose of this paper is to use finite element (FE) simulation to model the geometry of the test specimens and determine the temperature variation field in the material with a specified heat source location. By simulation it is more economy and

faster to test the best condition set for experiment. By this way, simulation could reduce cost and time wastage when it is advance into real experiment. FE analysis has been applied as a verification tool in some applications involving thermography. Louaayou *et al*⁽¹²⁾ applied a 2D finite element method to study the interaction of the specimen with the induction stimulation in an induction-lockin-thermography. Chaudhuri *et al*⁽¹³⁾ studied the defects in brazed joints through infrared thermography images and verified through FE simulation. A 3-D heat transfer model of a gear has been developed that has the ability to deal properly with heat flow though air filled cracks with openings in the micrometer range. This is achieved by balancing thermal fluxes flowing into the crack and through the crack, with those flowing out of the crack. There are several parameters considered in the simulation such as the crack size, gear material, and the temperature of the localised heat source. Each of these parameters affects the accuracy of the crack detection. Various shapes of defect were allocated in different locations from the heat source. The modelled 3-D gear was tested in different temperature conditions, different materials and smaller to bigger cracks to determine the best combination of their parameters which yield to better accuracy of the crack detection.

2. Specimen

The gear was modeled and the dimensions were indicated as in Figure 1. The modeled gears with 3mm and 6mm cracks around it are shown in Figure 2 and Figure 3 respectively. The modeled gears were then imported to Ansys software for finite element simulation. A heat source of 1cm cubic of volume was attached in between the gear teeth and axis rotation of the gear. The copper heat source was set to heat up to 200°C and the thermal conductivity was set at 386 W/m. °C.

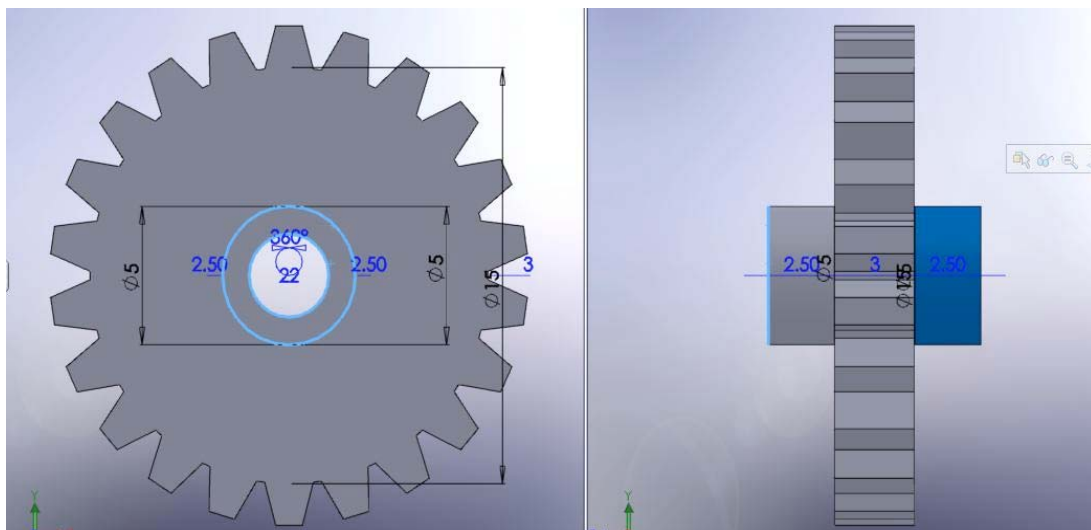


Figure 1. Gear model with dimensions.

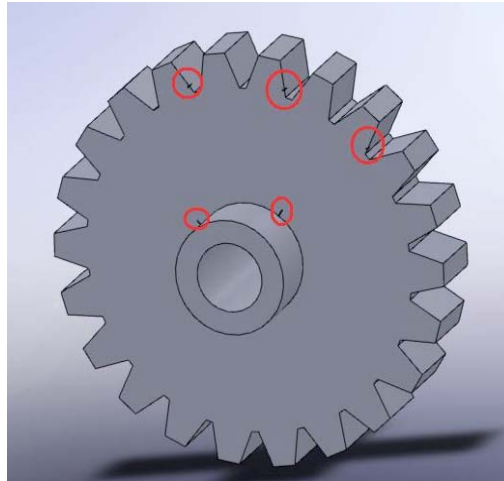


Figure 2. Gear model with 3mm cracks as marked in red circle

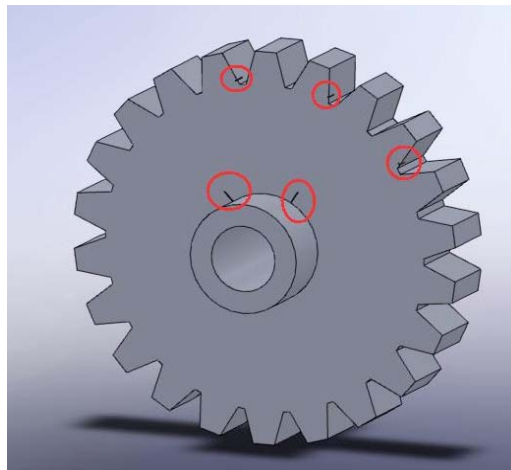
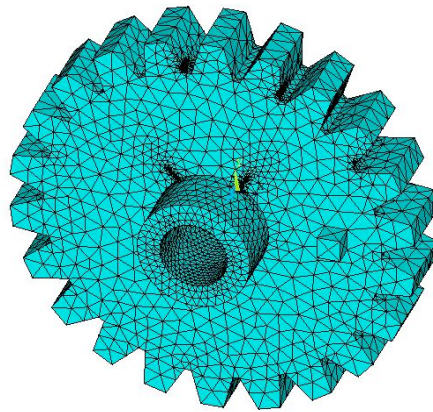


Figure 3. Gear model with 6mm cracks as marked in red circle

3. Experimental results

There are three types of gear material used for simulation of the 3mm cracks and 6mm cracks. They are medium carbon steel, aluminium alloy and nylon 66 40% carbon fibre filled composite gear. The gear model was meshed to smaller mesh as presented in Figure 4. The two types of heat loads namely conduction and convection were set in the finite element simulation. The heat source was set to generate heat up to 200°C. The convection film coefficient was set at 5 W/m²°C and the bulk temperature was set to 30°C. Figure 5 shows the conduction and convection loads configuration applied to the gear. The duration of simulation was set to 3600 seconds.



esktop\Solidworks document\gear8defect.x_t

Figure 4. Applied conduction and convection loads on gear

3.1 Simulation of medium carbon steel gear with 3mm and 6mm cracks

The material properties of medium carbon steel are shown in Table 1. Initially, the gear simulation was run in lesser number of sub-steps. Later, the simulations were run in more sub-steps. The gradual increase of the simulation iterations enhances the accuracy of the crack detection. The sub-step size can be regarded as the time divided by the number of step. Hence, this explains the sub-step size in the accuracy of the crack seizure in simulation. Figure 5 shows three simulations with different sub-step which represents different nodal temperature solutions in duration of 3600 seconds.

Table 1. Material properties of medium carbon steel

Properties:	Value:
Thermal Conductivity	36.9 W/m. °C
Specific heat	486 J/Kg. °C
Density	7820 Kg/m ³

PRINT TEMP NODAL SOLUTION PER NODE		PRINT TEMP NODAL SOLUTION PER NODE		PRINT TEMP NODAL SOLUTION PER NODE	
***** POST1 NODAL DEGREE OF FREEDOM LISTING *****					
LOAD STEP= 1 SUBSTEP= 100		LOAD STEP= 1 SUBSTEP= 300		LOAD STEP= 1 SUBSTEP= 600	
TIME= 3000.0 LOAD CASE= 0		TIME= 3000.0 LOAD CASE= 0		TIME= 3000.0 LOAD CASE= 0	
NODE	TEMP	NODE	TEMP	NODE	TEMP
1	128.76	1	128.99	1	129.05
2	127.50	2	127.74	2	127.80
3	135.40	3	135.61	3	135.66
4	142.33	4	142.52	4	142.57
5	128.84	5	129.07	5	129.13
6	128.94	6	129.17	6	129.23
7	135.36	7	135.56	7	135.62
8	135.78	8	135.98	8	136.03
9	135.83	9	136.03	9	136.08
10	143.26	10	143.44	10	143.49
11	128.88	11	129.11	11	129.16
12	127.55	12	127.79	12	127.85
13	130.33	13	130.56	13	130.61
14	129.42	14	129.65	14	129.71
15	127.58	15	127.81	15	127.87

Figure 5. Nodal temperature of sub-step 100, 300 and 600 at time=3000s

There are a total of 9058 nodal temperatures for each simulation of a given sub-step and time. Video simulations for each different sub-step were recorded. The nodal temperature result between first and second simulation shows a different temperature of less than 0.1°C while the results of second and third simulation shows temperature difference between 0.01°C to 0.09°C . The temperature difference is relatively small and can be ignored. Therefore, the solution is converging at the sub-step size of 5s. This means a further decrease of the sub-steps size will not show any difference in the solution but only increasing the computer calculating time. Therefore, the third simulation was convergence and only relevant data and results are taken. Simulations were done on the 3mm cracks on gear and 6mm cracks on gear. Figure 6 shows various heat distortions at temperature interval of 60°C - 90°C when it come into contact with 3mm cracks and 6mm cracks respectively in a duration of 3600s. On the other hand, Figure 7 shows heat distortion at temperature interval of 120°C - 150°C for 3mm cracks and 6mm cracks respectively. These simulations highlight the cracks detection and the form of heat distortion. The contour colour represents the interval temperature of 30°C and will further increase to 200°C .

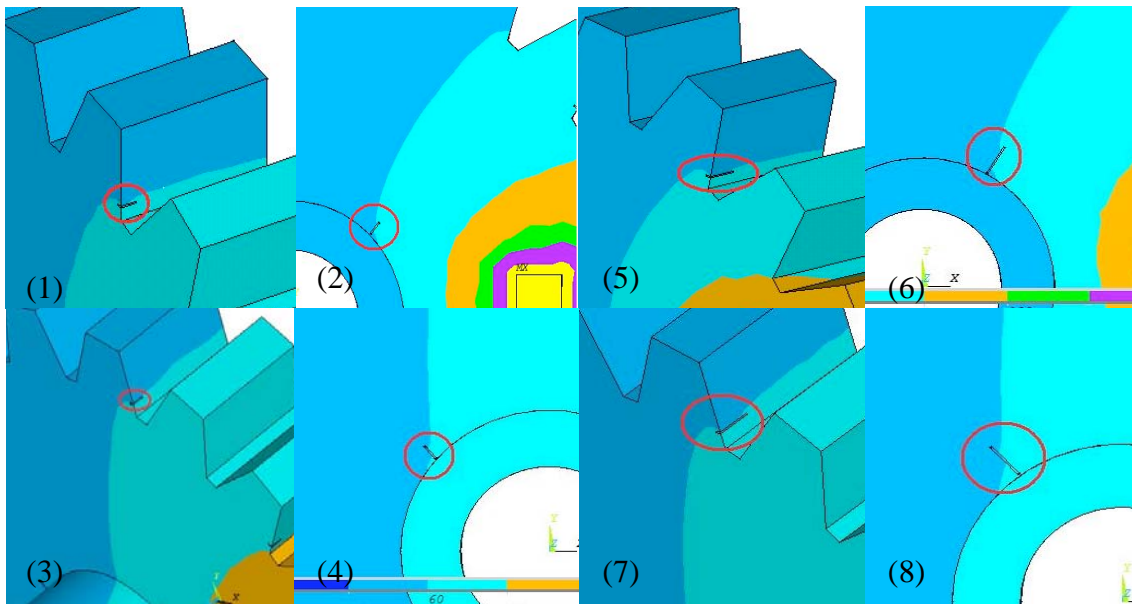


Figure 6. 60°C - 90°C heat distortion at 143s (1), 245s (2), 385s (3), and 618s (4) for 3mm cracks and heat distortion at 146s (5), 310s (6), 395s (7), and 610s (8) for 6mm cracks

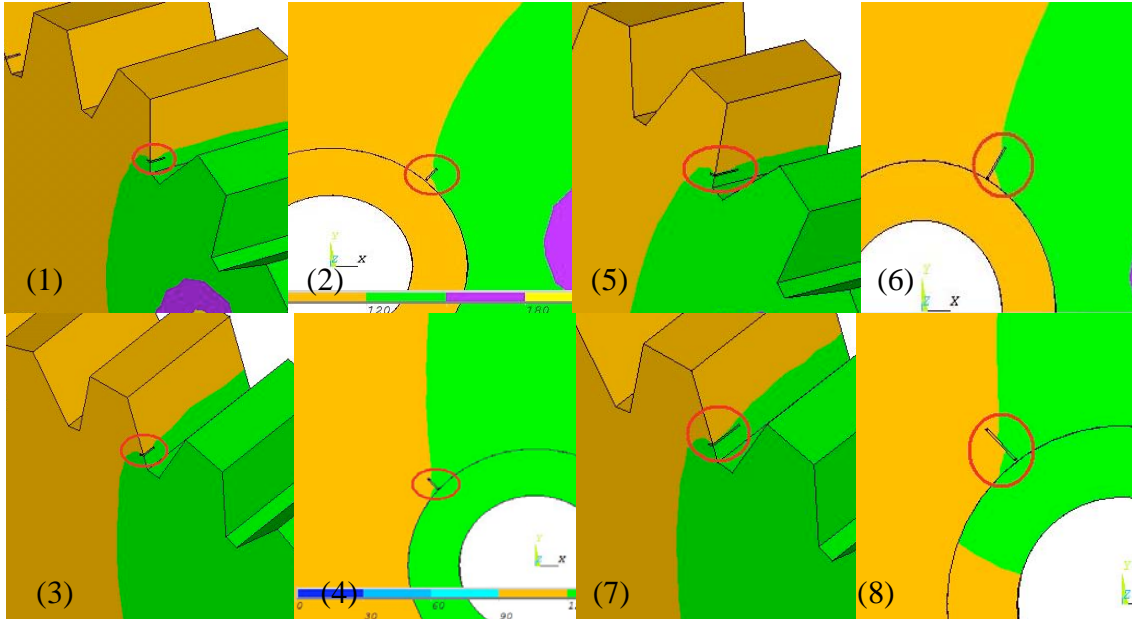


Figure 7. 120° C - 150° C heat distortion at 1226s (1), 1697s (2), 1968s (3), and 2407s (4) of 3mm cracks and heat distortion at 1268s (5), 1865s (6), 2020s (7), and 2420s (8) of 6mm cracks

The distorted heat path emphasizes the crack on this area. There are four different 3mm and 6mm cracks location as shown in Figure 6 and Figure 7. It shows the heat flow of 60°C-90°C, and 120°C-150°C temperature intervals distorts and emphasizes the cracks two times. As a remark, when the heat wave temperature increases, heat flows in a slower rate. This is due to the limit of thermal conductivity of the material that allows the heat flow through it. Thus, the heat wave in higher temperature is expected to detect cracks accurately since it needs more time for heat to propagate than the lower temperature heat wave.

3.2 Simulation of aluminium alloy gear with 3mm and 6mm cracks

The material properties of aluminium alloy gear are shown in Table 2. The thermal conductivity is much greater than the medium carbon steel. Figure 8 show the specimen reaches 200°C which is the steady state temperature in 1350 seconds. The simulation from 1350 seconds to 3600 seconds does not show any changes in the heat flow since the specimen is already in steady-state condition.

Table 2. Material properties of aluminium alloy

Properties:	Value:
Thermal Conductivity	151 W/m.°C
Specific Heat	915 J/kg.°C
Density	2470 kg/m ³

Since the simulation only shows result within 0 to 1350 seconds, the sub-steps are increased gradually in few simulations to enhance the accuracy of the result. Figure 9 shows the nodal temperature simulation for 1300 seconds duration. Simulations with 26

sub-steps and simulation with 130 sub-steps shows difference greater than 1°C, whereas the difference between simulation of 130 sub-steps and 260 sub-steps is roughly 0.3°C. Thus, simulation with 260 sub-steps is converging.

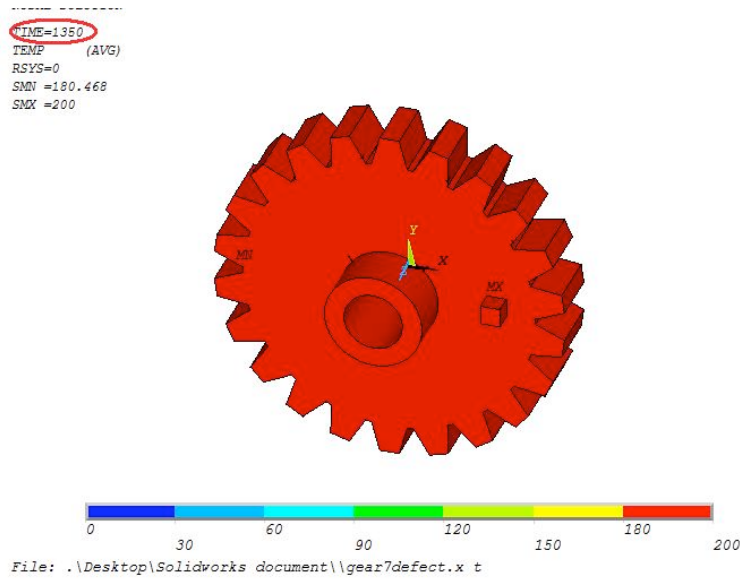


Figure 8. Gear in steady-state at time=1350s

LOAD STEP= 1 SUBSTEP= 26		LOAD STEP= 1 SUBSTEP= 130		LOAD STEP= 1 SUBSTEP= 260	
TIME= 1300.0	LOAD CASE= 0	TIME= 1300.0	LOAD CASE= 0	TIME= 1300.0	LOAD CASE= 0
NODE	TEMP	NODE	TEMP	NODE	TEMP
79	182.23	79	182.90	79	182.98
80	182.48	80	183.14	80	183.22
81	183.16	81	183.79	81	183.87
82	183.47	82	184.09	82	184.16
83	184.34	83	184.93	83	185.00
84	184.74	84	185.30	84	185.37
85	185.90	85	186.42	85	186.48
86	186.40	86	186.90	86	186.96
87	187.80	87	188.25	87	188.30
88	188.39	88	188.82	88	188.87
89	189.47	89	189.86	89	189.90
90	189.71	90	190.09	90	190.13
91	189.43	91	189.81	91	189.86
92	189.06	92	189.45	92	189.50
93	187.73	93	188.18	93	188.23
94	187.12	94	187.59	94	187.65
95	185.82	95	186.34	95	186.40
96	185.35	96	185.89	96	185.95
97	184.27	97	184.85	97	184.92
98	183.90	98	184.50	98	184.57

Figure 9. Nodal temperature of three simulations set at time 1300s

Figure 10 shows 180°C - 200°C heat distortion for 3mm and 6mm cracks respectively. The duration of the simulations were set to 1350 seconds.

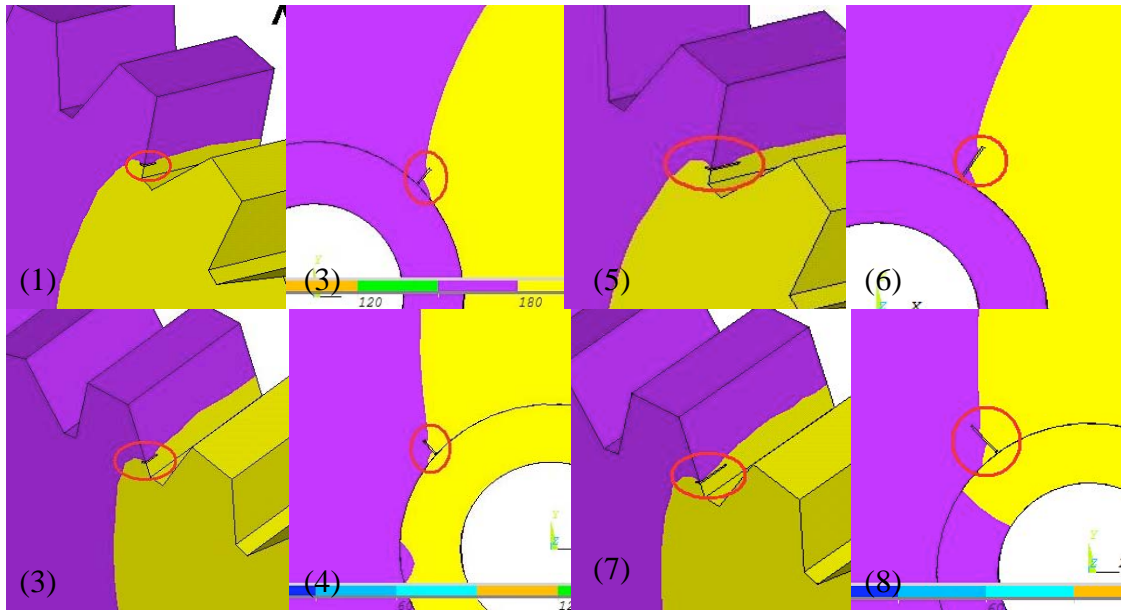


Figure 10. 180°C - 200°C heat distortion at 778s (1), 888s (2), 958s (3), and 1075s (4) of 3mm cracks and heat distortion at 801.7s (5), 944s (6), 986s (7), and 1095s (8) of 6mm cracks

The lower temperature interval below 180°C-200°C were difficult to be detected hence it was not included in the simulation. The heat propagates in a fast rate in the overall process. This is because heat propagates faster at lower temperature compared to higher temperature. Hence, time taken for heat to cross the cracks is also shorter and this makes it difficult to capture the heat distortion at that instant time.

3.3 Simulation of nylon 66, 40% carbon fiber filled composite gear with 3mm and 6mm cracks

Plastic gears are common to use in reduce the noise between the gears, light and low cost compared to alloy gear materials. Nylon also offers considerable toughness and wear resistance compared to other plastics used for gears. The purpose of choosing nylon 66 for simulation is due its low thermal conductivity. Therefore, it would be easy to determine the behaviour of the low conductivity behaviour with respect to the heat flow and heat distortion and to compare it with the previous tested materials used for gear. The material properties of nylon66, 40% carbon fibre composite were listed in Table 3.

Table 3. Material properties of nylon66, 40% carbon fibre composite

Properties:	Value:
Thermal Conductivity	4.90 W/m.°C
Specific Heat	1700 J/kg.°C
Density	1400 kg/m ³

Due to the relatively low thermal conductivity of nylon 66, the duration time of 3600 seconds is not sufficient to generate the crack detection simulation as shown in Figure

11. The temperature did not reach the temperature limit of 200°C in 3600 seconds. The heat distortion can only be found at 60°C-90°C intervals. To solve this, the duration is then increased to 7200 seconds in order to allow complete heating up to 200°C. Simulations at sub-step 70, 140, and 280 are as in Figure 12. The simulation with sub-step size of 25s is proved convergence. It has a small error different in the solution that can be ignored. Figure 13 shows the 60°C-90°C heat distortion for 3mm cracks and 6mm cracks, whereas Figure 14 shows the 90°C-120°C heat distortion for 3mm cracks and 6mm cracks respectively.

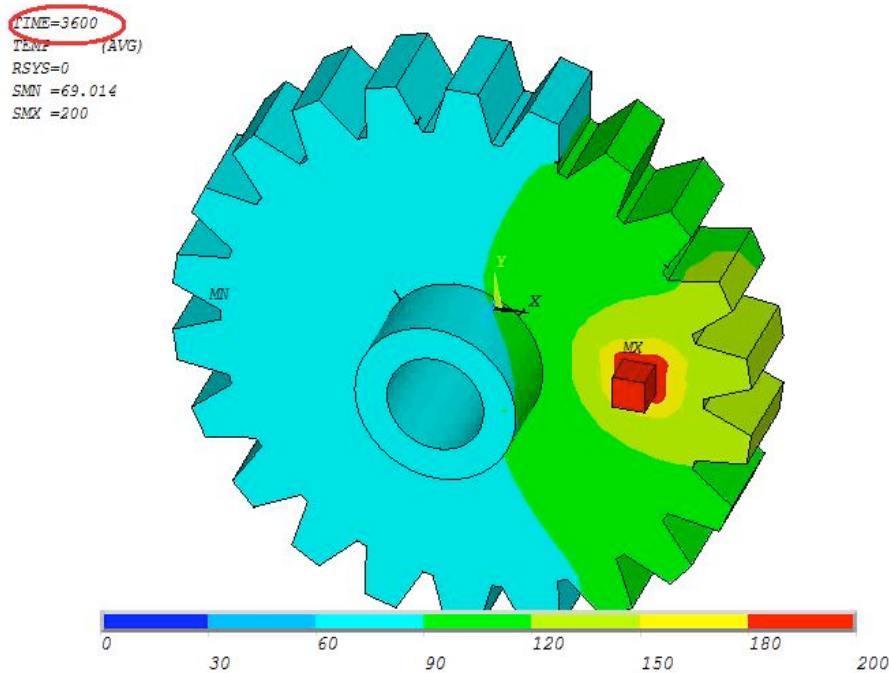


Figure 11. Simulation of the heat flow up to 3600 seconds

PRINT TEMP NODAL SOLUTION PER NODE		PRINT TEMP NODAL SOLUTION PER NODE		PRINT TEMP NODAL SOLUTION PER NODE	
***** POST1 NODAL DEGREE OF FREEDOM LISTING *****		***** POST1 NODAL DEGREE OF FREEDOM LISTING *****		***** POST1 NODAL DEGREE OF FREEDOM LISTING *****	
LOAD STEP= 1 SUBSTEP= 70		LOAD STEP= 1 SUBSTEP= 140		LOAD STEP= 1 SUBSTEP= 280	
TIME= 7000.0 LOAD CASE= 0		TIME= 7000.0 LOAD CASE= 0		TIME= 7000.0 LOAD CASE= 0	
NODE	TEMP	NODE	TEMP	NODE	TEMP
1	91.610	1	91.723	1	91.779
2	90.775	2	90.895	2	90.954
3	100.53	3	100.63	3	100.68
4	111.13	4	111.22	4	111.27
5	91.715	5	91.828	5	91.884
6	91.887	6	91.999	6	92.055
7	100.49	7	100.59	7	100.64
8	101.17	8	101.28	8	101.33
9	101.23	9	101.33	9	101.38
10	113.11	10	113.20	10	113.25
11	91.779	11	91.891	11	91.947
12	90.828	12	90.947	12	91.007
13	94.082	13	94.195	13	94.251
14	92.926	14	93.041	14	93.098
15	90.504	15	90.622	15	90.680
16	89.694	16	89.813	16	89.872

Figure 12. Nodal temperature of three different simulations set at time=7000s

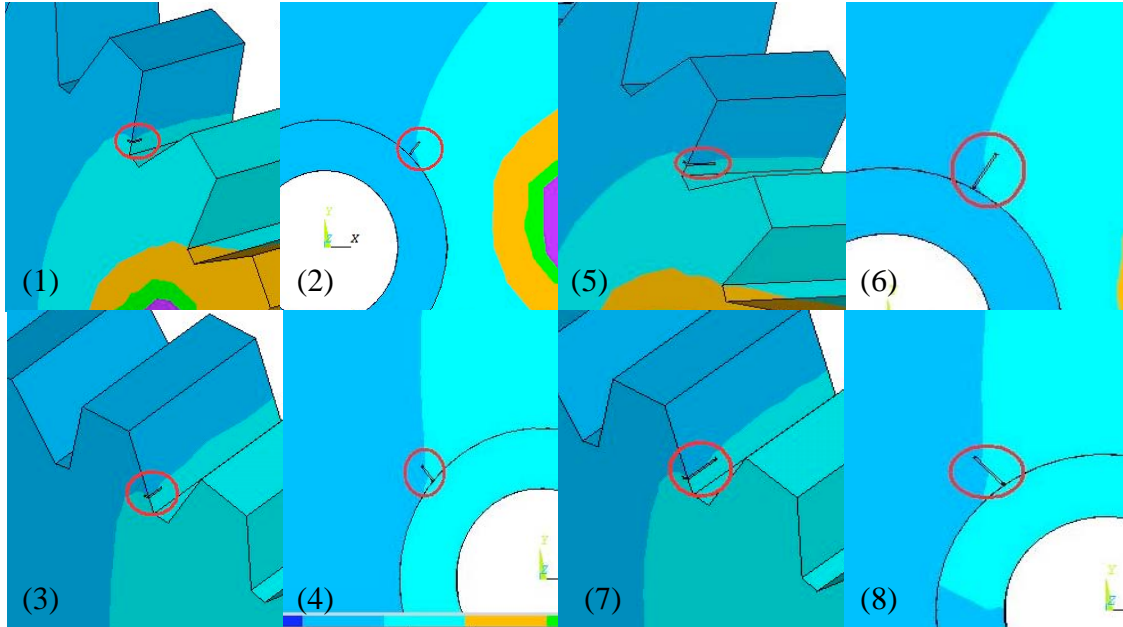


Figure 13. 60°C - 90°C heat distortion at 354s (1), 609s (2), 1020s (3), and 1700s (4) of 3mm cracks and heat distortion at time 362s (5), 810s (6), 1044s (7), 1670s (8) of 6mm cracks

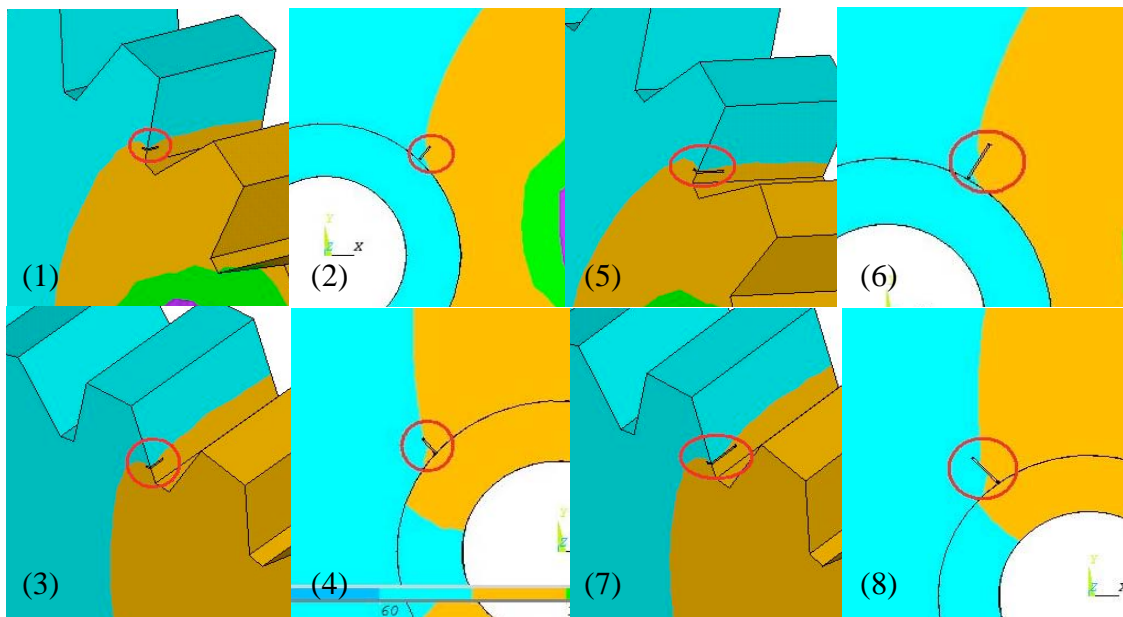


Figure 14. 90°C - 120°C heat distortion at 1274s (1), 2386s (2), 3461s (3), and 5800s (4) of 3mm cracks and heat distortion at time 1335s (5), 2944s (6), 3590s (7), and 5709s (8) of 6mm cracks

For material in lower thermal conductivity, it requires longer time for simulation. Compared to good conductor, the cracks are detected even in the low temperature wave; 60°C-90°C, the time to cross over the cracks is longer than good conductor. But not much heat layers could contribute in detecting the cracks as only small amount of heat could flow through the specimen.

4.0 Discussions

The experimental results were analyzed and studied. The results were categorized to four different factors that affect the heat flow and heat distortion across the cracks. Specifically, their factors that affect the heat flow in gear are the type of materials, crack size, temperature, and the crack location from the heat source.

4.1 Effect of heat propagation in different materials

Medium carbon steel gear has a moderate thermal conductivity of $36.9 \text{ W/m}\cdot\text{C}$. The heat conduction rate is moderately fast. It shows a good result, with 200°C in the duration of 3600s. Figure 15 shows in detail the heat propagation across the 3mm cracks. When the heat temperature increases, the heat flow slower and the cracks are detected accurately. Overall the data collected are sufficient with heat source of 200°C and 3600s in duration.

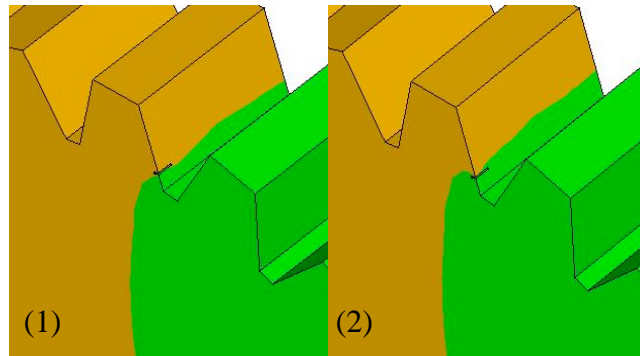


Figure 15. Heat flows propagates across 3mm crack at 1950s (1) and 1972s (2) of medium carbon steel

Aluminium has the highest thermal conductivity as it is a good conductor. Simulation shows that the aluminium gear reaches 200°C at 1350 seconds which is roughly half of the duration set at 3000 seconds. Since heat flows very fast, the cracks on the surface are not easily detected and a lower temperature heat flow tends to be even difficult to detect them. However, higher temperature heat wave tends to detect the cracks easily as shown in Figure 16.

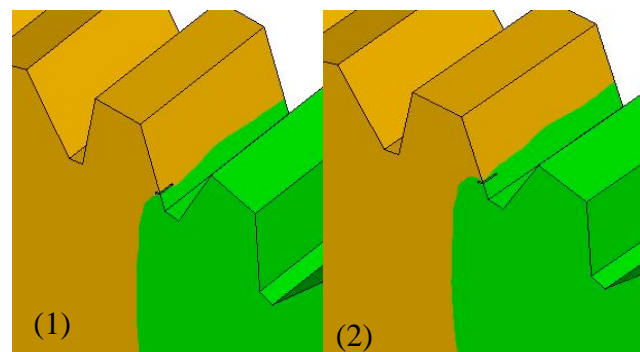


Figure 16. Heat flows across the 3mm crack at 241s (1) and 243s (2) of an aluminium gear

Heat distortion through crack in aluminium occurred rapidly compared to medium carbon steel. Time taken for heat flow across the crack of medium carbon steel was 22 seconds. The simulation shows that the crack was identified within 22 seconds where the heat path was distorted. In contrast, time taken for heat flow across the crack of aluminium gear was only 2 seconds. The higher the temperature, the longer time is required for heat to propagate. To enhance the results of the simulation, the heat source should be set at a higher temperature. Nylon 66, 40% carbon fibre filled composite has the lowest thermal conductivity. Compared to aluminium, nylon 66 requires longer time to reach maximum temperature of 200°C as shown in Figure 11. At 3600 seconds, heat flow at 60°C-90°C temperature interval did not propagate completely over the surface. Only two set of temperature intervals of 60°C-90°C and 90°C-120°C were able to show the results. The relative low thermal conductivity has reached its limit to further transfer the heat. Thus to further increase the heat flow on the surface, more energy is required. However, the maximum temperature for nylon 66 is about 250°C. Increasing the heat source's temperature is not a proper way as the specimen may undergo deformation. To overcome this problem, the temperature interval should be smaller. Selecting certain temperature region also allows the detection of heat distortion. For example, the temperature region 60°C to 120°C is the region which is of interest and the temperature display contour is set to smaller interval. These changes will yield to display lower temperature waves and show better results in simulation. Table 4 summarizes the problem and the solution to improve the selected materials respectively.

Table 4. Heat flow in different materials

Material	Conductivity	Problem	Solution
Medium Carbon Steel	Moderate	N/A.	A 200°C heat source in a duration of 3600 seconds is an optimum parameter
Aluminium	Good	At 200°C, heat flow in fast rate through cracks and is difficult to detect the crack by visualizing the heat distortion.	The higher the temperature, the greater the resistance to flow. Raising the temperature will extend the heat propagation time across the cracks. Therefore, easier to detect cracks.
Nylon66+carbon fiber	Poor	Nylon 66 is a good heat insulator. Therefore, only few temperature contours can be seen in the simulations.	Raising the temperature may deform nylon 66. The ideal temperature interval for nylon 66 was within 60°C to 120°C. Reducing the temperature contour may enhance the crack detection.

4.2 Heat flow across different crack size

The cracks are similar in width and depth but have different length. The shorter one is 3mm in length and the longer one is 6mm in length. From the simulations, the longer cracks requires more time for heat to propagate across it. This is due to the larger cracks gives greater resistance to the heat flow and lead to a longer time to propagate. This explains the heat distortion across the cracks. Figure 17 shows the time required for heat to propagate across the 3mm crack of medium carbon steel was roughly 107 seconds whereas Figure 18 shows the time required for heat to propagate across 6mm cracks of medium carbon steel was 140 seconds. Hence, this proved larger crack requires longer time for heat to propagate.

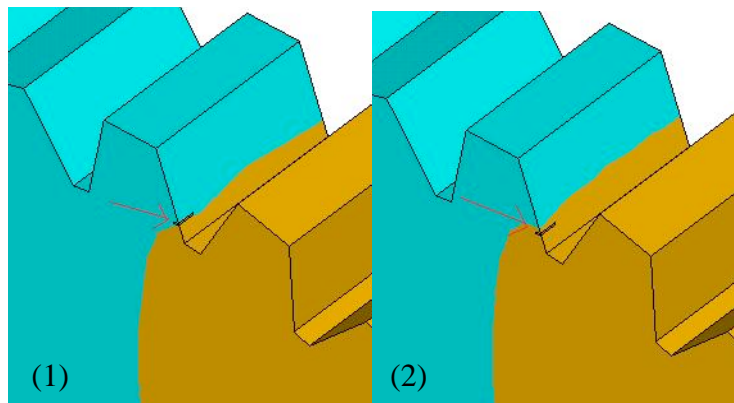


Figure 17. Heat flows across 3mm crack from 3373s (1) to 3480s (2)

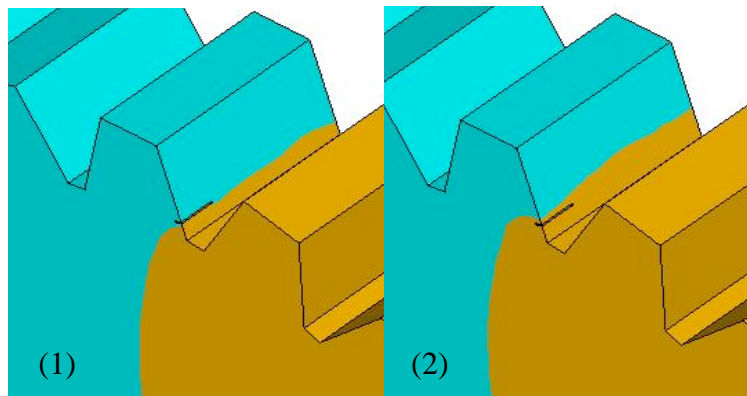


Figure 18. Heat flows across 6mm crack from 3470s (1) to 3610s (2)

4.3 Heat flows in different temperature intervals

Heat flows in different rate depending on the temperature from the heat source. Each temperature interval or called temperature range is represented in different contour colours. Each contour has different time interval when it flows across the crack. An increase in the temperature heat source leads to slower the heat propagation across the gear surface. Thus, it takes longer time to flows across the surface. Hence, it could detect smaller cracks. Figure 19 shows the time taken for heat to flow across the of 60°C-90°C interval was 10 seconds whereas Figure 20 shows the time taken for heat to flow across the crack of 120°C-150°C interval was 22 seconds. Time taken for each wave has a difference of 12s.

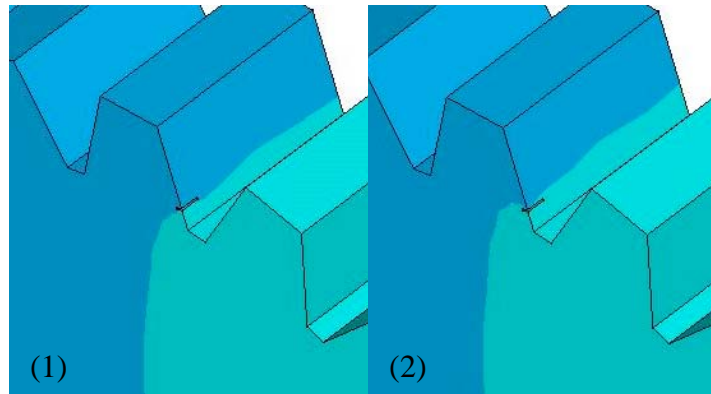


Figure 19. Heat flow of 60° C-90° C across the crack from 378s (1) to 388s (2)

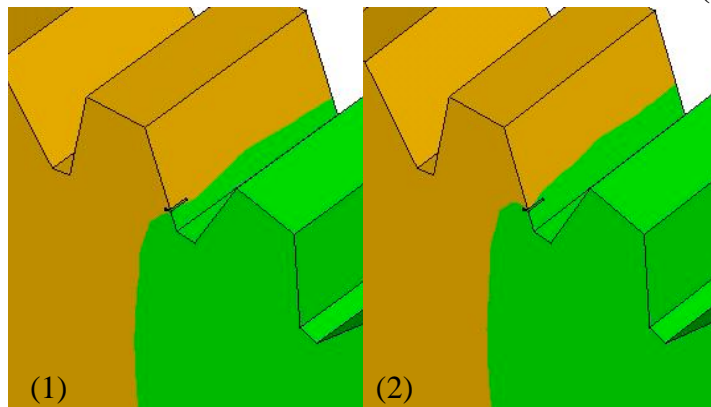


Figure 20. Heat flow of 120° C-150° C across the crack from 1950s (1) to 1972s (2)

As the temperature layer is increases, it leads to a slower propagation rate thus it could detect smaller crack as it flows slower over the surface. Similarly, when heat is applied to a good conductor material, lower temperature range is not suitable for the simulation since heat flows faster across the surface.

4.4 Crack position

The crack position from the heat source affects the rate of the heat flow across the gear surface. The rate of the heat propagation varies when it flows across cracks of different locations. The heat flow rate decreases when the crack position is further from the heat source. Heat flows at a slower rate when it is nearer to the heat source and flows faster when it is far from the heat source. Therefore, the cracks located near the heat source are easier to be detected compared to cracks located further away from heat source. Figure 21 to Figure 23 shows three different locations of the cracks on gear with respect to the heat source. The cracks in the figures were given the same crack size but differ in position. Time taken for the heat to flow through the cracks was calculated. The duration of the heat flow were recorded in Table 5. It was clearly seen in these figures that crack with the farthest distance from heat source takes only 5 seconds for heat to flow across it compared to crack closer to the heat source which takes about 10 seconds to flow across it.

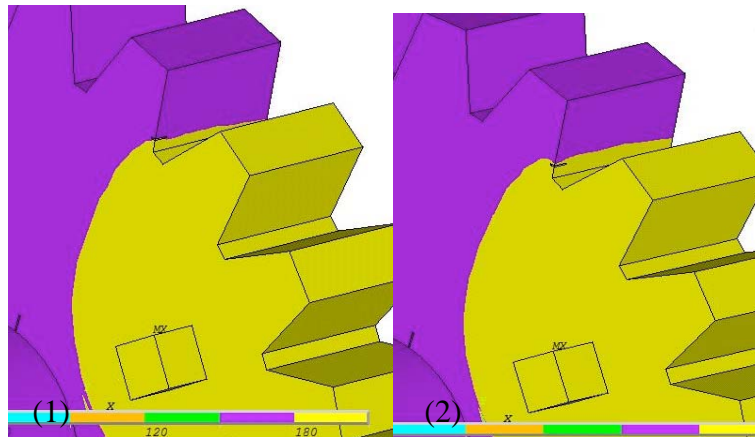


Figure 21. Heat flow across the first crack from 770s (1) to 780.5s (2)

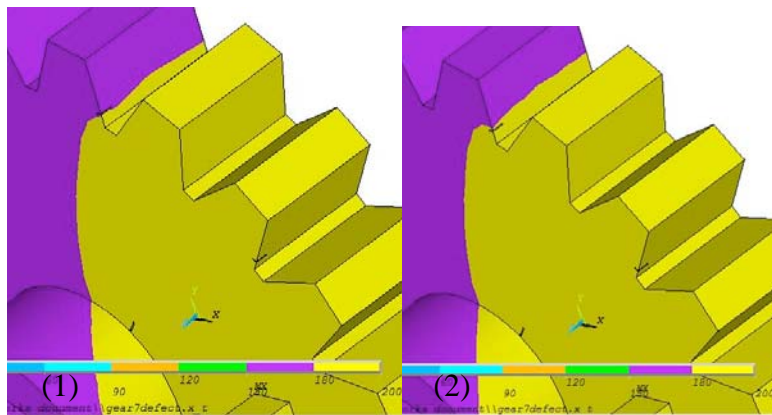


Figure 22. Heat flow across second crack from 953s (1) to 960s (2)

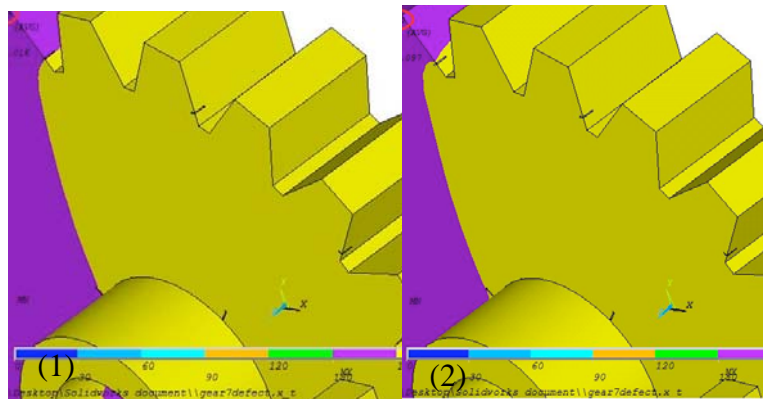


Figure 23. Heat flow across third crack from 1075s (1) to 1080s (2)

Table 5. Duration of heat flow propagation across different cracks location.

Crack	Heat flows enter time (second)	Heat flows leave time (second)	Duration (second)
1 (near)	770	780.5	15.5
2 (middle)	953	960	7
3 (far)	1075	1080	5

3. Conclusions

Finite element simulation of thermography on gear has been investigated. In particular, the crack detectability through heat distortion in gear has been investigated in relation with the different gear materials, the crack size, location of crack, and different temperature interval. Gear material of higher thermal conductivity shows that cracks were difficult to be detected under thermography simulation. Simulation of heat flow through gear also shows that gear with larger crack size is easier to be detected. When temperature interval of the gear increases, it leads to a slower propagation of heat flow through the gear. Hence, heat distortion takes place slower and was able to detect smaller crack as it flows slower over the surface. Cracks on gear which is located nearer to the heat source are easier to be detected compared to further ones.

References

1. F. Amon and C. Pearson, 'Thermal imaging in firefighting and thermography applications', *Experimental Methods in the Physical Sciences*, 43, pp 279-331, 2010.
2. D.J. Titman, 'Applications of thermography in non-destructive testing of structures', *NDT&E International*, 34(2), pp 149-154, 2001.
3. C. Meola, R. Di Maio, N. Roberti, and G.M. Carlomagno, 'Application of infrared thermography and geophysical methods for defect detection in architectural structures', *Engineering Failure Analysis*, 12(6), pp 875-892, 2005.
4. D.A. Haralambopoulos and G.F. Paparsenos, 'Assessing the thermal insulation of old buildings — the need for *in situ* spot measurements of thermal resistance and planar infrared thermography', *Energy Conversion and Management*, 39(1-2), pp 65-79, 1998.
5. C. Boué and D. Fournier, 'Cost-effective infrared thermography protocol for 40 μm spatial resolution quantitative microelectronic imaging', *Infrared Physics & Technology*, 48(2), pp 122-129, 2006.
6. J.M. Laskar, S. Bagavathiappan, M. Sardar, T. Jayakumar, J. Philip, and B. Raj, 'Measurement of thermal diffusivity of solids using infrared thermography', *Materials Letters*, 62(17-18), pp 2740-2742, 2008.
7. C. Meola, G.M. Carlomagno, A. Squillace, and A. Vitiello, 'Non-destructive evaluation of aerospace materials with lock-in thermography', *Engineering Failure Analysis*, 13(3), pp 380-388, 2006.
8. N.P. Avdelidis and D.P. Almond, 'Through skin sensing assessment of aircraft structures using pulsed thermography', *NDT&E International*, 37(5), pp. 353-359, 2004.

9. N.P. Avdelidis, B.C. Hawtin, and D.P. Almond, 'Transient thermography in the assessment of defects of aircraft composites', *NDT&E International*, 36(6), pp 433-439, 2003.
10. A. Levy, A. Dayan, M. Ben-David, and I. Gannot, 'A new thermography based early detection of cancer approach based on magnetic nanoparticles Theory simulation and in vitro validation (in press)', *Nanomedicine: Nanotechnology, Biology and Medicine*, doi:10.1016/j.nano.2010.06.007, 2010.
11. E.Y.-K. Ng, 'A review of thermography as promising non-invasive detection modality for breast tumor', *International Journal of Thermal Sciences*, 48(5), pp 849-859, 2009.
12. M. Louaayou, N. Naït-Saïd, and F.Z. Louai, '2D finite element method study of the stimulation induction heating in synchronic thermography NDT', *NDT&E International*, 41(8), pp 577-581, 2008.
13. P. Chaudhuri, P. Santra, S. Yoele, A. Prakash, D.C. Reddy, L.T. Lachhvani, J. Govindarajan, and Y.C. Saxena. 'Non-destructive evaluation of brazed joints between cooling tube and heat sink by IR thermography and its verification using FE analysis', *NDT&E International*, 39(2), pp 88-95, 2006.